Neuron, Vol. 46, 129–140, April 7, 2005, Copyright ©2005 by Elsevier Inc. DOI 10.1016/j.neuron.2004.12.057

Unitary IPSPs Drive Precise Thalamic Spiking in a Circuit Required for Learning

Abigail L. Person[1] and David J. Perkel[2,*]
[1]Graduate Program in Neurobiology and Behavior
University of Washington
Seattle, Washington 98195
[2]Departments of Biology and Otolaryngology
University of Washington
Seattle, Washington 98195

Summary

Song learning in birds requires a basal ganglia-thalamo-pallial loop that contains a calyceal GABAergic synapse in the thalamus. Information processing within this circuit is critical for proper song development; however, it is unclear whether activation of the inhibitory output of the basal ganglia structure Area X can drive sustained activity in its thalamic target, the medial portion of the dorsolateral thalamic nucleus (DLM). We show that high-frequency, random activation of this GABAergic synapse can drive precisely timed firing in DLM neurons in brain slices in the absence of excitatory input. Complex IPSP trains, including spike trains recorded in vivo, drive spiking in slices with high reproducibility, even between animals. Using a simple model, we can predict much of DLM's response to natural stimulus trains. These data elucidate basic rules by which thalamic relay neurons translate IPSPs into suprathreshold output and demonstrate extrathalamic GABAergic activation of thalamus.

Introduction

Calyceal synaptic terminals are specialized to convey temporally precise information by exerting exquisite control over postsynaptic conductances. The best-studied examples lie within ascending auditory pathways, where the preservation of precise spike timing is required for accurate sound localization (for review, see Trussell, 1999). Calyceal synapses accommodate one-to-one spike transmission (Guinan and Li, 1990), but to date, only glutamatergic synapses have been investigated for fidelity of information transfer (Zhou and Parks, 1992; Zhang and Trussell, 1994; Isaacson and Walmsley, 1995). The song-control system in songbirds (Figure 1A) features a calyx-like synapse that is GABAergic; each cell in DLM receives one, or at most two, axon terminals from the basal ganglia structure Area X (Luo and Perkel, 1999a; Luo and Perkel, 1999b). Like its glutamatergic counterparts, this synapse evokes large postsynaptic currents (Luo and Perkel, 2002), but it is unknown whether this input acts to drive or inhibit spiking in its target, DLM.

The anterior forebrain pathway (AFP; see Figure 1A) in oscine songbirds consists of three nuclei: Area X, DLM, and LMAN (lateral magnocellular nucleus of the anterior nidopallium), which together form a topographic loop required for song learning in juvenile songbirds and song plasticity in adults (Bottjer et al., 1984; Brainard and Doupe, 2000a; Luo et al., 2001). The AFP is thought to process sensorimotor information from HVC that propagates reliably through the circuit; neurons in HVC and LMAN show highly correlated activity, despite being separated by several synapses, including the calyx in DLM (Kimpo et al., 2003). How can temporally-precise song-related activity be transferred through DLM using an inhibitory synapse?

In mammals, pauses in tonic inhibitory input from basal ganglia output neurons (corresponding to Area X projection neurons) disinhibit targets in the thalamus (Deniau and Chevalier, 1985; Chevalier and Deniau, 1990). This disinhibition is associated with increased activity in thalamic target cells. Two primary hypotheses can account for this increased activity: gating excitatory input onto these cells, or directly driving postinhibitory rebound spikes. While these modes of basal ganglia-thalamic processing are not mutually exclusive, the former hypothesis has dominated models of thalamic relay of basal ganglia signals.

DLM receives only a sparse, presumably excitatory, projection from the motor nucleus RA and its surround (Wild, 1993; Vates et al., 1997; Foster et al., 1997). It is unclear to what extent these and other possible excitatory projections drive activity in DLM during singing-related behaviors. Importantly, spontaneous activity in RA does not clearly drive activity in DLM in vivo as shown by an uncoupling of RA and LMAN activity by HVC inactivation (Kimpo et al., 2003). In line with the anatomical specialization of the calyceal terminal from the basal ganglia in DLM, it is possible that GABA itself drives spiking in postsynaptic neurons via postinhibitory rebound. However, the mammalian literature provides several caveats pertinent to this hypothesis. In mammals, unitary IPSPs can be very weak in the thalamus (under 1 mV at –63 mV rest; Kim et al., 1997) and therefore insufficient to induce postinhibitory rebound. Also, the generation of rebound spikes is slow (Thomson, 1988; Bal et al., 1995; Ulrich and Huguenard, 1997b) and therefore might not be suited to relay temporally precise information. These findings have led to broad doubts of whether extrathalamic GABAergic inputs could drive activity in the thalamus (Sherman and Guillery, 1998; Sherman and Guillery, 2001).

To address these issues, we took advantage of the one-to-one presynaptic to postsynaptic cell arrangement to define the input-output characteristics of an inhibitory forebrain synapse involved in a learned behavior. We report that high-frequency, Poisson trains of unitary IPSPs can induce reproducible, precisely timed postsynaptic spiking during the IPSP barrage. In addition, natural stimulus trains recorded from putative Area X projection neurons in vivo reliably drove rebound spiking in DLM. We used a simple model to estimate the spiking response to these natural trains. Taken together, the results suggest that postinhibitory rebound

*Correspondence: perkel@u.washington.edu

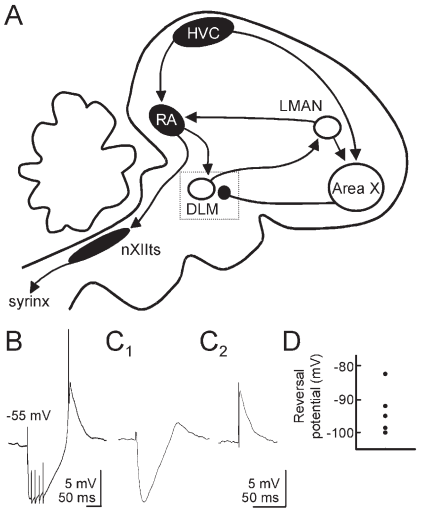

Figure 1. Extrathalamic Inhibitory Projection to the Thalamus of Songbirds

(A) Schematic diagram of oscine song-system anatomy. Open nuclei represent the anterior forebrain pathway Area X → DLM → LMAN, which process sensorimotor information from HVC. The box highlights the inhibitory synaptic connection between Area X and DLM investigated in this study.

(B) Example of postinhibitory rebound following a brief 100 Hz barrage of IPSPs induced by tetanic stimulation of the afferent. Note the compound sodium and calcium spike.

(C) Example of a unitary IPSP recorded in perforated-patch configuration, with the pipette containing 37 mM Cl^- (C_1). Upon break-in, the $GABA_A$ receptor-mediated PSP became depolarizing (C_2). All IPSP experiments were carried out in the presence of 10 μM CNQX. Vrest = –55 mV.

(D) Distribution of reversal potentials in perforated-patch configuration. Note their considerable negativity.

can facilitate translation of complex IPSP trains into temporally precise rebound spikes.

Results

We used whole-cell or gramicidin-perforated patch recording to measure postsynaptic membrane potential in response to synaptic stimulation in DLM neurons from adult male zebra finches in an acute brain slice preparation. Stimulation of Area X inputs to DLM evoked large, unitary (all-or-none) IPSPs, which could drive a characteristic rebound spike burst, consisting of a broad calcium spike crowned with one or more sodium spikes. As has been observed previously, Figure 1B illustrates a typical response to a short train of IPSPs (Luo and Perkel, 1999a). Sodium spikes could be discriminated from calcium spikes by their short duration (0.5 ms width at half-maximal amplitude versus >5 ms width at half-maximal amplitude, respectively). After achieving stable intracellular recordings, we screened for IPSPs; subsequently, all experiments were carried out in the presence of 10 μM glutamate receptor antagonist 6-cyano-7-nitro-quinoxaline-2,3-dione (CNQX). Unless noted, errors indicate SEM.

Native Chloride in DLM Neurons Renders IPSPs Hyperpolarizing from Rest

Previous reports of the Area X → DLM synapse were almost completely limited to whole-cell recordings, which likely influenced intracellular chloride concentration. For rebound-driven spiking to be a plausible mechanism for information transfer through DLM, it was important to know whether IPSPs are hyperpolarizing with native chloride concentration. We therefore recorded from cells in the perforated-patch configuration, where the pipette solution contained high [Cl^-] (37 mM), which upon intentional patch rupture would render $GABA_A$ receptor-mediated IPSPs depolarizing from rest (–32.1 mV calculated reversal potential). We could thus distinguish between undisrupted and disrupted patch conditions. Under these conditions, unitary IPSPs were strongly hyperpolarizing (Figure 1C_1). Short (30–50 ms) 100 Hz trains of stimuli evoked rebound spikes. After patch rupture, IPSPs became depolarizing within 1 min (Figure 1C_2, n = 3). In experiments with 9–10 mM Cl^- in the pipette, the measured $GABA_A$ reversal potential was extremely negative in both recording configurations (–93.6 ± 3.5 mV, n = 5, perforated patch, [Figure 1D]; –89 ± 6.7, n = 7, whole cell; see Experimental Procedures). Thus, under conditions that maintain native chloride, IPSPs are of sufficient amplitude to induce rebound spikes in DLM neurons.

High-Frequency Poisson Trains of Unitary IPSPs Evoke Rebound Spiking

We were ultimately interested in understanding the patterns of unitary IPSPs that could give rise to rebound spiking in DLM neurons. To this end, we stimulated axons from the basal ganglia structure Area X with Poisson stimulus trains (Berger et al., 1987), which lack patterned structure and thus permit calculation of an unbiased spike-triggered average. Each stimulus train consisted of 3 s of stimuli at a mean rate of 140 Hz, which is within the range of firing rates reported for putative Area X projection neurons (Hessler and Doupe, 1999; Margoliash, 1997). We then analyzed the patterns of synaptic activity that gave rise to rebound spikes.

DLM neurons were quiescent prior to Area X afferent stimulation (mean RMP = –54.6 mV; SD 2.8, n = 10). Each Poisson train strongly and persistently hyperpolarized the cell; however, at certain points in the train, rebound spikes shot transiently above baseline (Figure 2A). Rebound spiking was sustained throughout the IPSP train (Figure 2B), thus vesicle depletion or receptor desensitization do not limit the capacity for prolonged periods of rebound firing. We analyzed the translation of these trains into spiking by determining the pattern of stimuli that preceded each rebound spike (Figure 2C), which we used to calculate a rebound spike-triggered average (Figure 2D). Only rebound events that included a sodium spike were analyzed (Figure 2A, inset).

In the stimulus raster plot (Figure 2C), each row corresponds to a rebound spike, which occurred at t = 0; each tick mark represents one stimulus to the afferent fiber. Raster plots for stimuli preceding all rebound events in each cell were pooled into a histogram (i.e.,

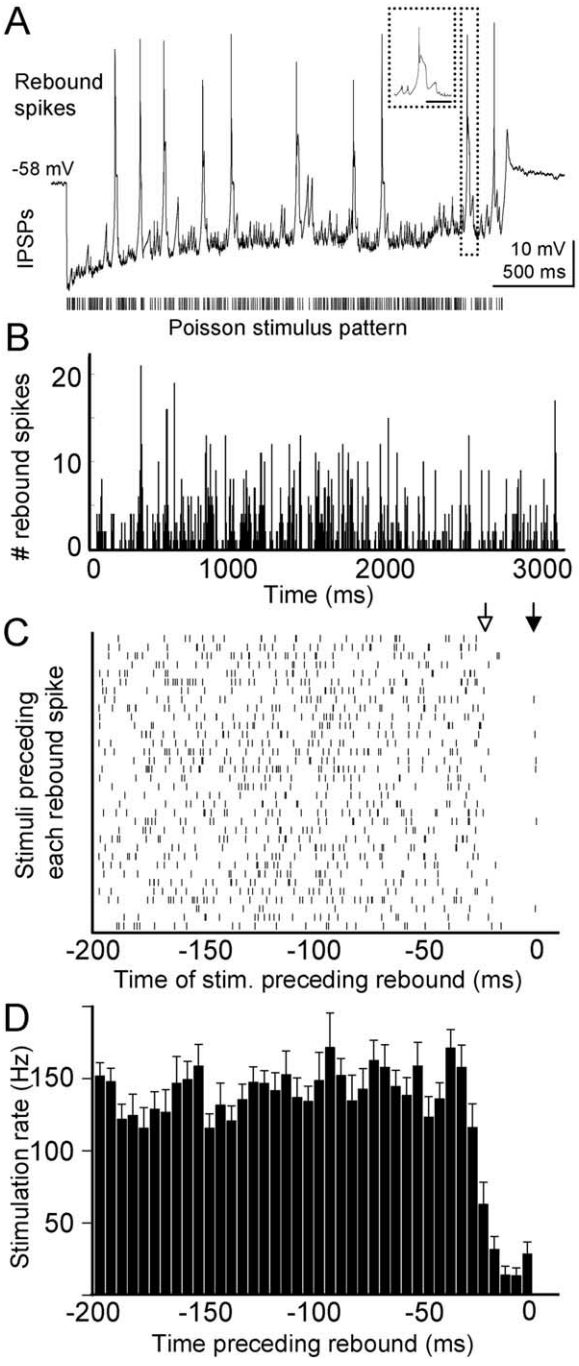

Figure 2. Rebound Spikes Are Elicited during High-Frequency, Poisson IPSP Trains

(A) Perforated-patch recording of a DLM neuron in the presence of CNQX illustrating the response to a Poisson train of unitary IPSPs, evoked by stimulating the GABAergic afferent to the DLM neuron. The pattern of stimuli is illustrated below the voltage trace as a series of tick marks. Stimulus artifacts have been shortened. Inset illustrates a fast sodium spike riding on a broader calcium spike (inset; scale = 50 ms).

(B) Histogram of rebound spike times for all cells and all trains illustrating sustained rebound responses to the random trains.

(C) Raster plot of IPSP trains for one cell, aligned to the rebound spike time (t = 0). Each tick represents a *stimulus* delivered to the GABAergic afferent. Each row contains the stimuli that precede each postsynaptic rebound spike (34 shown). A precipitous drop in the likelihood of occurrence of stimuli (open arrow) was evident approximately 25 ms before the rebound event (closed arrow).

(D) Summary data for stimuli preceding rebound spikes for ten cells. Histogram of stimulus rate preceding all rebound events for all cells. Error bars plot SEM; bin size = 5 ms. Note the pronounced deviation of the histogram at time points close to zero from the flat average rate of 140 Hz, indicating that consistent stimulus features give rise to rebound events across cells.

the spike-triggered average, Figure 2D) which represents the average rate of the stimulus train prior to each rebound spike. There was a relatively uniform rate of stimuli between 200 ms and 30 ms prior to the rebound spike. The histogram plateaued at the average stimulus rate of 140 Hz during this period (Figure 2D, n = 10, 139.12 ± 2.7 Hz). However, 20 ms prior to each rebound spike, there was a marked decrease in the stimulus rate. This decrease appears as a gap in the raster plot immediately prior to t = 0 (Figure 2C, arrows) and as a marked deviation in the histogram. Stimulus rate in the 20 ms prior to rebound was 14.3 ± 3.1 Hz (n = 10). A few stimuli occurred within 5 ms prior to the rebound event. In these cases, the stimulus was delivered after the spike was initiated but was insufficient to abort the spike. The step-like shape of the spike-triggered stimulus average suggested that thalamic neurons can act as feature detectors, responding to long interstimulus intervals in complex, high-frequency trains of IPSPs.

IPSPs Can Drive Sustained Firing at Rates over 10 Hz, Despite Low Spike-Transfer Efficiency

We analyzed the statistics of stimulus-interval sensitivity by measuring the size of the stimulus interval flanking each rebound spike (Figure 3A). The design of the Poisson trains meant that there were many short stimulus intervals and few long stimulus intervals (Figure 3A, dotted bars). Rebound spike probability was greater for longer stimulus intervals, although these long intervals occurred less frequently (Figure 3A, compare solid and dotted bars). For example, each neuron that encountered a stimulus interval over 70 ms responded with rebound spikes. (Only one cell received a train with a stimulus interval between 60 and 70 ms, and it did not generate a sodium spike, accounting for the gap in the histogram in Figure 3A.)

We also observed that the interspike interval histogram recapitulated the exponential decay in the frequency of long stimulus intervals in the Poisson stimulus train (Figure 3B). This distribution argues against classical thalamic oscillatory activity (McCormick and Pape, 1990) during the IPSP trains. Two distinct peaks were clear in the interspike interval histogram: the first, with very short interspike intervals (<4 ms) represented multispike bursts riding on broader depolarizations. Spiking in these bursts occurred at rates over 250 Hz. The second peak was centered around 120 ms and fell off exponentially. Together, the average rate of rebound events during the train was 2.45 ± 0.67 Hz (n = 10 cells).

Overall, the rebound spike rate was far lower than the stimulus rate of the inhibitory afferent. We quantified the input-output relationship by calculating the spike-

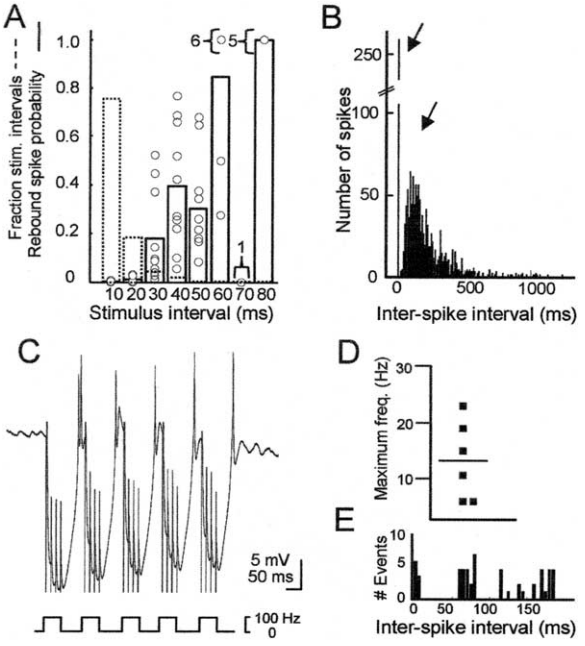

Figure 3. Input Rate Filtering at Area X to DLM Synapse

(A) Two overlayed histograms showing the probability of rebound spikes as a function of interstimulus interval in the Poisson train (solid line bars) and the fraction of interstimulus intervals in the Poisson trains that were of a particular size (dashed line bars). The likelihood of rebound spiking increased with longer interstimulus intervals. Open circles represent per-cell measurements.

(B) Histogram of interspike intervals for rebound events driven by Poisson trains (bin size = 5 ms). The prominent peak at very short ISIs represents spikes within bursts.

(C) An example of entrainment of rebound spikes with repeated pauses in an IPSP train. DLM neurons showed reliable rebound spikes in response to repeated, short barrages of IPSPs. A rebound spike was elicited during each long stimulus interval. Vrest = –53 mV.

(D) Distribution of maximum rates elicited with short IPSP barrages as shown in (C). Cells could be driven at an average rate of 13 Hz with such a stimulus.

(E) Interspike interval histogram for cells driven maximally by patterned IPSP trains shown in (C) and (D).

transfer efficiency of the synapse as defined by the rate of rebound spikes generated divided by the average stimulation rate. The mean spike-transfer efficiency across cells was 0.017 ± 0.005 (n = 10 cells), indicating over a 50-fold decrease from the input rate of 140 Hz. This low spike-transfer efficiency indicates that there was substantial filtering of the input rate in these experiments.

The result that DLM neurons respond reliably to long stimulus intervals that nonetheless occur infrequently led us to ask whether the low efficiency value was due to a limit in the cell's ability to produce rebound spikes (i.e., refractoriness) or due to suboptimal stimulus statistics (i.e., infrequent long stimulus intervals). Thus, we next attempted to drive rebound spikes at higher rates with patterned stimulus trains. We used a stimulus train interspersed with pauses, spaced to drive each cell optimally (see Experimental Procedures). Rebound spikes reliably occurred during repeated pauses within the IPSP train (Figure 3C), such that unitary IPSPs consistently drove the postsynaptic cell at rates over 10 Hz (mean: 13 Hz, range: 6–23 Hz, Figure 3D, n = 6). Outside of short interspike intervals contained within bursts, interspike intervals were never shorter than 50 ms, an indication of the long refractory period of the low-threshold spike that underlies rebound (Figure 3E). Across cells, the rebound spiking was 3.9-fold below the average input rate of 50 Hz, for a spike-transfer efficiency of 0.26 ± 0.06 (n = 6), 15-fold greater than seen with Poisson trains. This value represents an upper bound to the rate of sustained IPSP-driven rebound spiking. The range of efficiency values observed suggests that the statistics of the stimulus train in large part determine the input-output rate relation at this synapse.

Short-Term History Dependence of Rebound Spike Latency

Neural activity propagates between HVC and LMAN (the target of DLM projections) in approximately 60 ms (Kimpo et al., 2003). Long delays through the thalamus have been hypothesized to account for much of this delay (Luo and Perkel, 1999b). To explore more thoroughly the extent to which DLM introduces a delay in the propagation of activity through the AFP, we measured the latency of the rebound spike with respect to the onset of the pause in the Poisson train experiments (Figure 2C, open arrow). Across cells, rebound latencies ranged from 20 to 86 ms during the train, with a mean of 29.15 ± 0.9 ms (n = 10). A cumulative distribution plot of all rebound latencies illustrates a broad range in each cell (Figure 4A). These values provide an estimate of the delay introduced in Area X → DLM spike relay at the synapse.

We next explored the stimulus parameters that influence rebound latency. Because of a body of research on the currents that underlie postinhibitory rebound, namely I_T and I_h, (McCormick and Pape, 1990; Lüthi et al., 1998; Porcello et al., 2003), we predicted rebound latency was both time and voltage dependent. We delivered constant-frequency (100 Hz) IPSP trains between 50 and 500 ms long (Figure 4B; enlarged, right) and measured the latency from the last stimulus of the train to the first rebound spike (Figure 4C). The rebound latency was consistently shorter following longer trains (R^2 = 0.98 ± 0.005, n = 13, fitted single exponential decay). We also held each cell at 2 membrane potentials with DC injection during synaptic stimulation. Rebound latency was significantly longer at –65 mV than –55 mV (Figure 4C, p = 0.001, paired Student's t test, n = 13). Thus, we observed short-term history dependence of rebound spike latency that was also influenced by the steady-state membrane potential.

To further link IPSP-driven rebound spike latency with I_T and I_h, we analyzed the membrane voltage at several points in the sweep and correlated these measurements with rebound latency. We measured the maximum and minimum voltage during the train, which will influence both currents, and also the amplitude of the depolarizing sag during each train due in part to I_h. The hyperpolarization maxima and minima occurred near the onset and terminus of the train, respectively; the minimum hyperpolarization occurred at the final

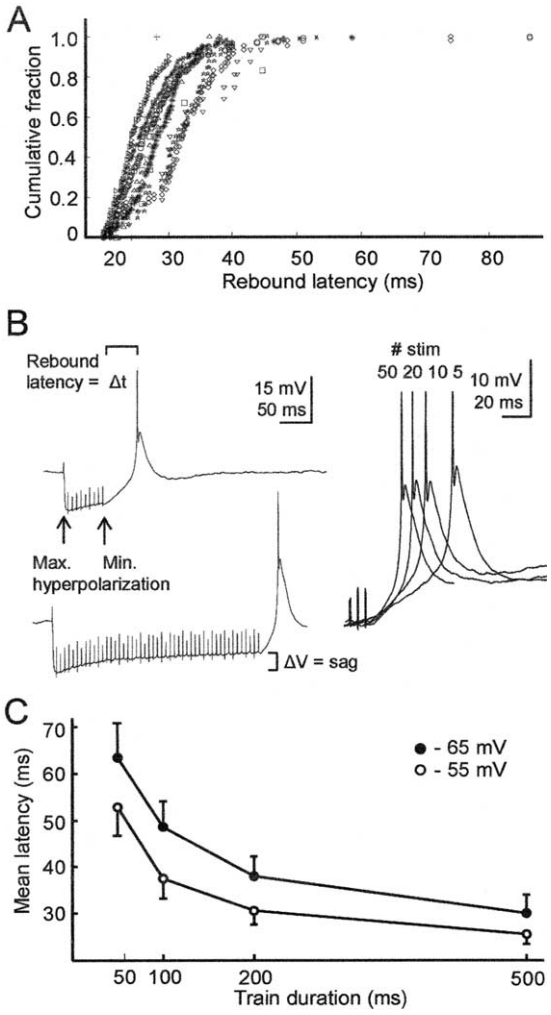

Figure 4. Rebound Latency Was Influenced by Duration of IPSP Trains

(A) Cumulative fraction plot illustrating range of rebound spike latencies observed during Poisson trains for each cell (indicated with different symbols).

(B) Whole-cell recording of a DLM neuron illustrating rebound from 100 Hz IPSP trains of different lengths (top, 100 ms; bottom, 500 ms). (Right) Overlay of four rebound spikes aligned to the final stimulus, arising from trains of IPSPs with varied numbers of stimuli, indicated above each trace. The rebound latency following a 50 stimulus train is shorter than that following a 5 stimulus train. Vrest = –58 mV.

(C) Summary of rebound-latency data for 13 cells. The rebound latency was negatively correlated with train length, which was systematically varied between 50 and 500 ms at 100 Hz. Cells were held with DC injection at two different membrane potentials prior to stimulus onset. Bars indicate SEM.

IPSP due to the depolarizing sag during sustained trains of IPSPs (Figure 4B, arrows). The sag amplitude was defined as the difference between the maximum and minimum voltage.

The amplitude of sag over the course of the train was significantly correlated with rebound latencies in each cell (R^2 = 0.58 ± 0.07, n = 13, range: 0.8–8.8 mV). The maximum hyperpolarization of the cell was less predictive of rebound latency, with significant linear correlations in just 4 of 13 cells (R^2 = 0.21 ± 0.05, n = 13, range: –65.4 to –80.7 mV). The membrane potential at the terminus of the train was significantly correlated with rebound latency in 10 of 13 cells (R^2 = 0.41 ± 0.08, n = 13, range: –79.9 to –60.4 mV).

Thus, as would be predicted from voltage- and current-clamp studies in other species (Coulter et al., 1989; McCormick and Pape, 1990), time- and voltage-dependent conductances influence rebound timing. The amplitude of the depolarizing sag during the hyperpolarization appears to account for a greater proportion of rebound-latency variability than any other single factor.

Temperature Dependence of Rebound Spike Latency

We tested the effect of temperature on rebound spike latency and found that in all cells tested, rebound after 100 Hz trains was accelerated at warmer temperatures; rebound latency was significantly shorter at 32°C compared to 28°C (paired Student's t test, $p < 0.05$, n = 6). For example, the rebound latency after a 200 ms, 100 Hz train was accelerated from 22 ms at 28°C to 14 ms at 32°C. We included temperature effects from a variety of stimulation parameters in the paired analysis. To capture the temperature dependence of rebound latency, we calculated the temperature coefficient Q_{10} for each cell. The mean Q_{10} was 2.6 ± 0.23 (n = 5), which is similar to that seen in rat thalamus for I_T (Coulter et al., 1989). The extrapolated rebound latency for a 200 ms 100 Hz train at avian body temperature of 41°C was 8.9 ± 3.4 ms (n = 5), indicating the potential for shorter delays through thalamus than previously appreciated (Luo and Perkel, 1999a; Dave and Margoliash, 2000; Kimpo et al., 2003). Throughout our experiments, we paid close attention to bath temperature to minimize variability due to temperature in our rebound-latency measurements (see Experimental Procedures).

Thalamic Neurons Detect Changes in IPSP Rates

The results of the Poisson-train experiment suggested that only brief pauses in IPSP arrivals were required to elicit rebound. If a pause of only 20–25 ms was sufficient to trigger rebound spiking, moderate frequency trains (20–50 Hz) might be expected to elicit rebound spikes repeatedly between each IPSP. However, such moderate frequency IPSP trains did not drive rebound spikes during the train: 50 Hz IPSP barrages effectively inhibited the cell until termination, at which point a rebound spike occurred. However, if a higher frequency priming train preceded a 50 Hz train of IPSPs, a rebound spike was elicited at the transition between high and moderate stimulation frequencies (Figure 5A).

We investigated this phenomenon systematically by delivering a 100 Hz train of IPSPs to each cell for several hundred milliseconds, which was then stepped to lower frequencies between 70 and 20 Hz. Rebound spikes were consistently generated at the transition between high- and low-frequency IPSPs. We term these rebound spikes "transition" spikes. We noted the frequency at which transition spikes were elicited in each cell (Figure 5B). Six of eight cells generated transition rebound spikes at 50 or 40 Hz. The mean latency from

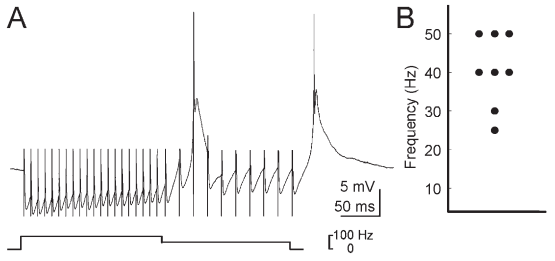

Figure 5. Rebound Spikes Occur at IPSP Frequency Transitions during a Train

(A) Perforated-patch recording of a DLM neuron in which a 100 Hz IPSP train was stepped to 50 Hz. A rebound spike was elicited after the transition from 100 to 50 Hz. Vrest = –60 mV.

(B) Summary data for eight cells in which IPSP train frequency was modulated in a stepwise manner. Each point represents one cell. The ordinate represents the maximum IPSP frequency at which a rebound spike was elicited after step reduction of stimulus frequency from 100 Hz.

the time of the final priming stimulus to the peak of the transition spike was 43.9 ± 10.5 ms. Thus an interstimulus interval of 20–25 ms, if preceded by shorter interstimulus intervals, can be detected as a "pause," eliciting rebound.

Poisson Trains Drive Rebound Spiking Deterministically within Cells

If the timing of rebound spikes is in fact dictated by low-threshold spike refractory period (Figure 3), train duration (Figure 4), and frequency transitions (Figure 5), then random trains of IPSPs could be expected to evoke rebound spikes deterministically; i.e., rebound spikes should occur with precise timing between duplicate presentations of a single random train. To test this idea, we presented each Poisson train twice to the cell. Voltage records were remarkably similar between presentations (Figure 6A, top and bottom traces); both sub- and suprathreshold features were reproducible. We focused our analysis on the timing of suprathreshold rebound spikes evoked with duplicate Poisson train presentation. A raster plot of spikes elicited during each pair of stimulus trains illustrates the high degree of response precision across trials (Figure 6B).

To quantify the relationship of rebound spike times between train presentations, we performed cross-correlation analyses (see Experimental Procedures). Across within-cell pairs, the mean peak cross-correlation coefficient (CCF) was 0.71 (SD 0.16) at a median lag of 1 ms (Figure 6C). These peaks were significantly greater than CCFs for shuffled data (mean peak = 0.18 [SD 0.15], median lag = 0 ms, $p < 0.001$, paired t test, n = 8 cells; 53 train pairs). The width at half-height of the CCF was 10 ms, which can be regarded as an estimate of the jitter over the course of the entire train. Over shorter intervals, repeated presentations of Poisson trains elicited rebound spikes that in many cases occurred within 1 ms of each other. These data indicate that IPSPs, though hyperpolarizing, can drive precise spiking in these cells.

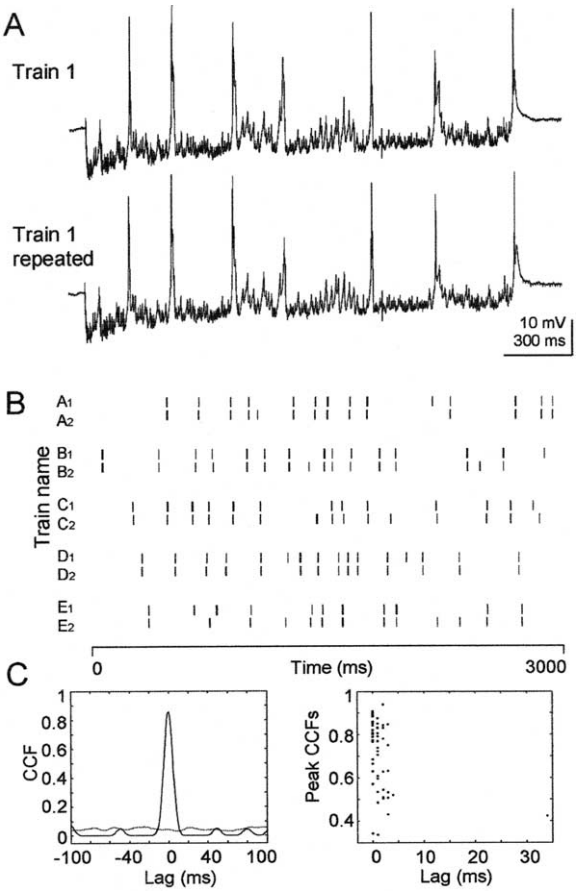

Figure 6. Poisson IPSP Trains Drive Rebound Firing Deterministically within a Cell

(A) Two example traces of DLM recordings (perforated patch) in which a Poisson IPSP train was delivered to the cell in duplicate. Both rebound spikes and subthreshold membrane potential trajectories were almost identical between the two iterations. Vrest = –57 mV.

(B) Raster plot of rebound spikes in a different cell. Each Poisson train was presented in duplicate. Each sodium spike in a rebound burst elicited during the train is represented by a raster tick. Note precision of spike times for many trains.

(C) (Left) Example of typical cross-correlation function. Note the peak at zero lag. The shuffled cross-correlation is flat and indicated with a dashed line. (Right) Summary of cross-correlation analysis with peak correlation coefficient plotted against location of peak (lag).

Poisson Trains Drive Rebound Spiking Reproducibly between Cells

We next investigated the input-output characteristics of DLM neurons as a population. Since responses to Poisson trains were reproducible within a single cell, we wondered whether responses to duplicate Poisson trains generalized across cells. We presented the same Poisson trains to cells from different animals (n = 8 cells; 342 train pairs). Across cells, responses to duplicate trains were highly similar, though more variable than within a single cell (Figure 7A). Rebound spike times aligned in a raster plot in many cases with submillisecond precision (Figure 7B). Cross-correlation analysis revealed CCFs with minimal lag in most comparisons, with a mean peak CCF of 0.37 (SD 0.12) and

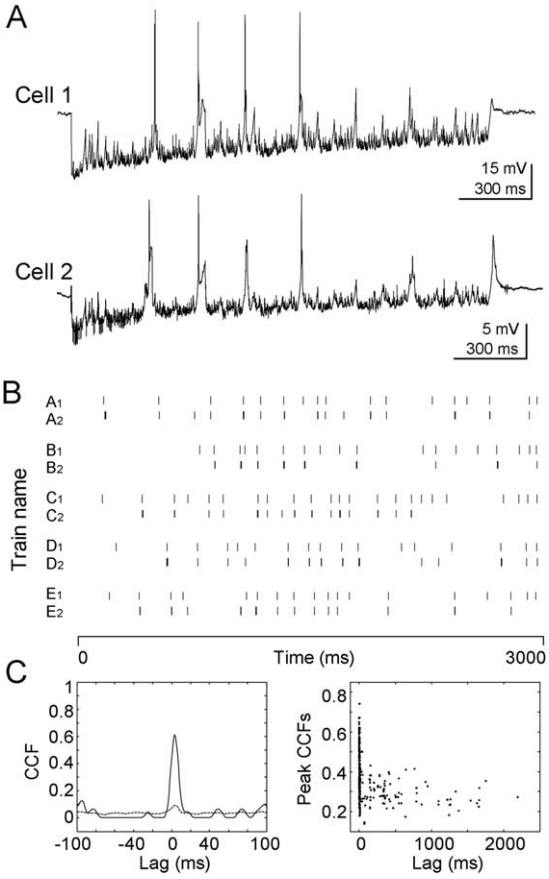

Figure 7. Poisson IPSP Trains Elicit Rebound Spiking Reproducibly between Cells

(A) Example responses of two DLM neurons from different animals to identical Poisson IPSP trains. Note that rebound spikes are elicited at the same point in the train for each cell. Top trace, Vrest = –53 mV; bottom trace, Vrest = –58 mV.

(B) Between-cell rebound spike raster plot. Pairs of rows represent the same train delivered to different cells. Note considerable similarity in rebound times between cells to the same Poisson train. Each pair illustrated was stimulated with a different stimulus train.

(C) (Left) An example cross-correlation function. Shuffled CCF is indicated with a dashed line. (Right) Summary of cross-correlation analysis with peak correlation coefficient plotted against location of peak.

median lag of 7 ms (Figure 7C). The width at half-height was 14 ms. The mean peak CCF was significantly greater than the mean shuffled peak (mean peak: 0.21 [SD 0.07], median lag: –397 ms; $p < 0.001$, paired t test, n = 342 train pairs).

Even when spike mismatches occurred, subthreshold rebound events (Ca^{2+} spikes not accompanied by Na^{+} spikes) were often noticeable in the membrane voltage of the cell that did not spike, perhaps owing to differences in resting membrane potential or spike threshold. These results suggest that different DLM neurons use similar rules to translate patterns of IPSPs into suprathreshold output.

Natural IPSP Stimulus Patterns Drive DLM Rebound Spiking

We next asked whether natural spike trains could also evoke rebound spiking, as would be predicted if Area X employs a rebound mechanism to propagate information through DLM. We used three different trains recorded in Area X in vivo: two trains recorded from the same neuron in response to repeated playback of a bird's own song (BOS) to an anesthetized zebra finch (Figure 8A, provided by S. Kojima and A.J. Doupe, UCSF) and one recorded during singing from a different animal (provided by N.A. Hessler and A.J. Doupe, UCSF). We refer here to the playback-derived trains as BOS-based IPSP trains, bearing in mind that BOS refers only to the individual bird in which the stimulus train was recorded and not those used in our in vitro slice preparation containing the DLM neurons we recorded.

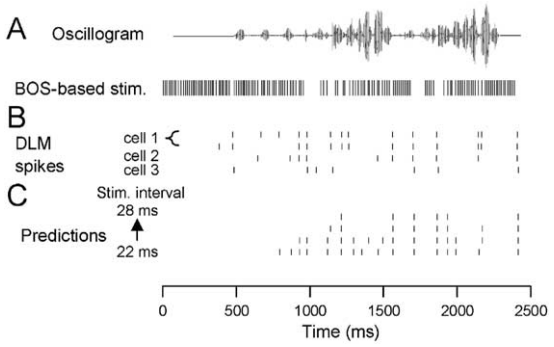

Figure 8. Rebound Spikes in Response to Natural Stimulus Patterns and Linear Predictions of Spiking

(A) Oscillogram of bird's own song (BOS) and single unit activity recorded in Area X evoked by song playback in the anesthetized zebra finch (S. Kojima and A.J. Doupe, personal communication). These spikes were converted into a stimulus train and used to activate the GABAergic afferents from Area X to DLM in the slice.

(B) Raster plot of rebound spikes from three DLM neurons in response to stimulation of afferents with this natural spike train. The top row represents spiking in the absence of CNQX; the bottom three rows are in the presence of CNQX.

(C) Predictions of rebound spiking in response to the natural spike train: four sets of predicted spikes in which interstimulus intervals of a particular duration threshold were used to predict the occurrence of rebound spiking.

Presentation of each BOS-based IPSP train elicited precisely timed rebound spikes (Figure 8B, n = 5), occurring at long stimulus intervals in the train. Within-cell cross-correlations of rebound spikes elicited with a single BOS-based IPSP train had a mean peak CCF of 0.63 (SD 0.18, n = 25 pairs) and a width at half-height of 8 ms.

Spike times differed in response to the two BOS-based trains, (within-cell mean peak CCFs comparing data for two trains were significantly decreased: 0.37 [SD 0.11, $p < 0.001$]). These data suggest that while DLM neurons are capable of responding with precise timing to a repeated train, they are sensitive to the precision of the input train, resulting in spike-time variability due to slight changes in the temporal patterns of inputs. The mean firing rate from rebound spikes in response to the two BOS-based trains was 3.5 ± 1.0 Hz (n = 5 cells) and 3.9 ± 1.2 Hz (n = 4 cells), respectively, for a mean spike-transfer efficiency of 0.046 ± 0.01. Thus, when analyzed over larger time windows there was little difference in the rate of rebound spiking in

response to the two BOS-based IPSP trains. Finally, the pattern of rebound spiking was not altered by CNQX. In the absence of antagonist rebound responses were very similar (mean peak CCF = 0.68 [SD 0.07], n = 8 train pairs, Figure 8, top row of raster ticks in cell 1). In two cells that received both Poisson trains and BOS-based spike trains, spike-transfer efficiency varied between the two inputs (means: 0.04 versus 0.075, respectively).

We also used a stimulus train recorded from a single unit in Area X in the singing animal (Hessler and Doupe, 1999). In response to this train, rebound spiking was precise but very sparse (within-cell mean peak CCF = 0.84 [SD 0.14], median lag = 1 ms, n = 5 cells, 5 train pairs, spike-transfer efficiency = 0.0035). As predicted from results of the Poisson train experiment, rebound spikes occurred after long stimulus intervals. These results indicate that DLM can respond precisely to input trains collected under different behavioral states in vivo.

Predictions of Rebound Spiking to Natural Stimulus Trains

We interpreted the spike-triggered average (Figure 2C) to suggest that DLM neurons detect a pause in the arrival of IPSPs (i.e., a long stimulus interval). We scanned the stimulus train for stimulus intervals of a particular threshold length and constructed a predicted spike train based on when those intervals occurred (Figure 8C). For example, if we scanned for an interval length of 24 ms, all intervals 24 ms and longer would be tagged and a rebound spike predicted after a 29 ms rebound latency (Figure 4A). We repeated this analysis for stimulus interval lengths ranging from 12 to 32 ms and finally applied a 50 ms refractory period to the predicted trains. We then analyzed the set of predicted spikes by (1) calculating the correlation coefficient between model spiking and observed spiking and (2) calculating the percent of observed spikes in each cell predicted by the model.

The raster plot illustrates that the predictions captured the basic structure of the observed rebound spikes (Figure 8C). The mean cross-correlation from each set of predicted spike trains with all observed spike trains was 0.36 (SD 0.12). When we allowed the interval threshold to vary between cells, to match each cell's rebound spike rate, we predicted 63% (SD 23%, n = 5) of observed spikes within 15 ms. Predictions made with a stimulus interval of 22 ms matched the average observed rebound spike rate.

Peak CCF values for the predicted and observed spikes were not significantly different from between-cell peak CCF values for BOS-based IPSP trains (0.37 [SD 0.001], n = 10 pairs; p = 0.74; Student's t test). The percent of spikes predicted by between-cell pairs for responses to BOS-based trains was also not significantly different from the predictions (64% [SD 28%], n = 10 pairs, p = 0.95; Student's t test). Thus, these predictions were as accurate as could be expected based on between-cell variability. With this method there was a systematic failure to predict rebound spikes that occurred very early in the train, further suggesting a time-varying condition that permits rebound spiking. Future studies could include other prediction approaches, including conductance-based models, to thoroughly characterize nonlinear dynamics that specifically control rebound spike generation and timing.

Discussion

We have shown that high-frequency trains of unitary IPSPs can drive activity in thalamic relay neurons. The GABAergic calyceal synaptic terminal from the basal ganglia structure Area X can preserve spike-timing information, despite relying on a rebound mechanism in the postsynaptic thalamic neuron. This finding provides a mechanism whereby song-related activity in the anterior forebrain pathway can propagate reliably, even through an "inhibitory" projection. More broadly, our data suggest a role for postinhibitory rebound firing in response to extrathalamic GABAergic input (Sherman and Guillery, 2001). While GABAergic circuitry can maintain thalamic oscillations, postinhibitory rebound is not appreciated as a mechanism for preservation or relay of precise spike-timing information. Our data show that thalamic neurons can translate GABAergic basal ganglia input into precise, nonoscillatory postsynaptic firing in a circuit essential for learning.

Our experiments were designed to explore general properties of GABAergic processing in the thalamus. To this end we attempted to create relatively realistic in vitro conditions. First, because only a single Area X afferent contacts each DLM neuron, bulk electrical stimulation can activate a unitary input. We thus avoided the potential problem of unrealistic simultaneous activation of a population of afferent fibers. Second, by using gramicidin-perforated patch recording, we maintained the native chloride concentration, ensuring accurate polarity and amplitude of IPSPs. As in mammalian thalamic neurons, we also observed quite negative IPSP reversal potentials, which may be required for $GABA_A$ receptor-mediated burst firing (Ulrich and Huguenard, 1997a; Ulrich and Huguenard, 1997b). Third, although we used pharmacological blockade of glutamate receptors to ensure isolation of the IPSP, antagonists were not necessary to evoke rebound spiking in response to high-frequency IPSP trains. These data also argue against widespread excitatory collateral circuitry within DLM that would have been activated by rebound firing in DLM neurons other than the one recorded.

IPSP Feature Detection

Though DLM neurons can detect long interstimulus intervals in high-frequency trains of IPSPs (Figure 2), not every long interval elicited a rebound spike (Figure 3A). Because the refractory period of low-threshold spikes underlying rebound is long (150 ms for complete recovery; Jahnsen and Llinas, 1984a; Jahnsen and Llinas, 1984b), the ability of the cell to follow pauses in high-frequency trains is limited. This partly accounts for the low efficiency values observed (ratio of output spike rate to stimulus rate). The spike-transfer efficiency for sustained IPSP trains had a maximum value of 0.26 as shown with patterned trains (Figure 3C). The efficiency for Poisson trains and natural trains was 6- to 15-fold lower, indicating a dynamic range in efficiency that

could be utilized at this synapse to alter the overall spike rate in DLM.

The finding that Poisson trains elicit rebound spiking with precise timing between presentations (Figures 6 and 7) suggests that DLM translates IPSPs into suprathreshold output using a deterministic mechanism. We used the step-like spike-triggered stimulus average as a guide to quantitatively predict thalamic output in response to a natural spike train input (Figure 8). Predicted rebound spike trains were well-correlated with the experimentally observed rebound spikes. Correlation coefficients for observed spikes between cells were similar to those comparing predicted and observed spikes, thus our predictions are as good at accurately predicting a cell's responses as the variability between individual cells permits.

Our model failed to predict all spikes, suggesting that a model incorporating nonlinearities, such as a conductance-based model, will better suit this system. In addition, mechanisms underlying between-cell variability in response to complex IPSP trains could be explored on a per-cell basis. The range of rebound spike latencies (Figure 4) illustrates nonlinearities that were not captured in the simplified model we used. Nevertheless, over half of observed spikes can be accounted for by using a very simple model. For this linear behavior, the rules for translating IPSP input into rebound spike output can be summarized very simply as a stimulus interval of at least 20 ms during a high-frequency IPSP barrage, and a requirement of at least 50 ms (Figure 3) before another long stimulus interval can elicit the next rebound spike.

Implications for the Song System

Numerous lines of evidence indicate that the anterior forebrain pathway (AFP) plays a crucial role in song learning and adult plasticity in oscines (Bottjer et al., 1984; Scharff and Nottebohm, 1991; Sohrabji et al., 1990; Williams and Mehta, 1999; Brainard and Doupe, 2000a; Brainard and Doupe, 2000b). The AFP processes auditory information related to the bird's own song (Doupe and Konishi, 1991) and has been hypothesized to use this information to guide motor plasticity (Brainard and Doupe, 2000b). In addition, the AFP shows activity during singing, even in deafened animals, indicating that motor-related signals are also present (Jarvis and Nottebohm, 1997; Hessler and Doupe, 1999). Activity in LMAN was recently shown to lock to song output with <2 ms precision (Leonardo, 2004). Regardless of the specific role of the AFP, it is clear that it can maintain temporally precise spike transmission across several synapses (Kimpo et al., 2003), though it was unclear how the strongly hyperpolarizing GABAergic projection from Area X to DLM could support propagation of this activity.

We used spike trains recorded in Area X as stimulus patterns for DLM neurons, under the assumption that they represent the activity of projection neurons that would synapse on DLM neurons. We have several reasons to believe this assumption is reasonable. The pallidal-like projection neurons of Area X are thought to be spontaneously active at high rates and to pause in response to inhibitory inputs from spiny neurons in Area X (Farries et al., 2005; Farries and Perkel, 2002). In fact, activity consistent with this scheme has been observed in vivo during singing (Hessler and Doupe, 1999) and during song playback (Margoliash, 1997; S. Kojima and A.J. Doupe, personal communication). The activity of the Area X units used for synaptic stimulation in this study contain these features, thus we believe they are to date the best candidates for the projection neurons.

In terms of Area X processing, inhibitory input from striatal cells and excitatory input from pallial cells (HVC, LMAN) modulate the tonic activity of the pallidal-like projection neurons (Farries et al., 2005). Projection neurons in the song nucleus HVC burst sparsely during singing (Hahnloser et al., 2002) and may contribute to shaping the pauses that we have shown can directly drive spiking in DLM neurons (Figure 8). In this way, DLM neurons can read-out specific features of tonically active pallidal-like cells, if not "add" new information. Our data do not, of course, rule out the possibility that Area X could gate extrinsic excitatory inputs into DLM, which may render DLM a center for processing information from other areas. Nevertheless, Area X-driven activity in DLM provides a plausible mechanism for information transfer within the AFP, even in the absence of concurrent glutamatergic synaptic activity.

While the specific arrival times of IPSPs determine postsynaptic spike timing, rebound spike rate over long intervals, reflecting the efficiency, depends on the overall statistics of the input train. For example, we observed variability in the rebound spike times, but not overall rebound spike rate, between responses to each BOS-based IPSP train. As we learn more about sensorimotor processing in the song system as well as general rules of neural encoding in the thalamus, it will be interesting to compare the degree to which temporal and rate codes are important in the function of these circuits.

Applicability to Mammals

Because the Area X → DLM synapse is unusual in its size and strength, it is reasonable to ask whether our data are compatible with pallido-thalamic connections in mammals. While no comparable study has, to our knowledge, been done in slices to investigate the functionality of pallido-thalamic GABAergic synapses, experiments in vivo suggest there are unequivocal inhibitory roles of these inputs in mammals (Ueki, 1983; Deniau and Chevalier, 1985). From these studies it is difficult to discern whether bursts occurred during periods of tonic pallidal activity, thus they do not rule out an additional driving role of GABAergic afferents. In fact, mammalian pallidal neurons form dense terminal plexi on motor thalamus neurons (Parent et al., 2001), reminiscent of the calyx in DLM.

From a more cellular perspective, random white-noise current injections elicit precise spiking from mammalian pyramidal neurons and neurons of the deep cerebellar nuclei (Mainen and Sejnowski, 1995; Gauck and Jaeger, 2000), and complex stimulus trains can activate highly reproducible currents in mammalian hippocampal neurons (Dobrunz and Stevens, 1999). Future studies should investigate to what extent this mode of thalamic relay may be utilized in mammalian basal-ganglia-thal-

amic circuitry. We hypothesize that our results will generalize to at least some regions of mammalian thalamus because of the high degree of conservation of vertebrate brain structures.

Experimental Procedures

Animals

A total of 26 adult male zebra finches (*Taeniopygia guttata*) were used in this study. Birds were obtained from commercial suppliers, and procedures were approved for use by the University of Washington Institutional Animal Care and Use Committee. Birds were housed on a 13:11 hr light/dark cycle in groups of five or fewer. Food and water were available ad libitum.

Slice Preparation

Methods used were similar to those detailed in Stark and Perkel (1999). Briefly, birds were anesthetized with isoflurane and decapitated. The brain was rapidly dissected and immersed in ice-cold, oxygenated artificial cerebrospinal fluid (ACSF) containing 119 mM NaCl, 2.5 mM KCl, 1.3 mM $MgSO_4$, 1 mM NaH_2PO_4, 16.2 mM $NaHCO_3$, 2.5 mM $CaCl_2$, 11 mM D-glucose, and 10 mM HEPES, osmolarity 285–295 mOsm, pH 7.2. Parasagittal brain slices (350–400 μm) were cut with a vibrating microtome then transferred to warm (35°C–40°C) ACSF with HEPES replaced by equimolar $NaHCO_3$. Slices were stored submerged in ACSF continuously bubbled with a gas mixture of 95% O_2 and 5% CO_2 for at least 1 hr prior to use.

Electrophysiological Recording

Blind, whole-cell (Blanton et al., 1989), or gramicidin-perforated patch recordings were made from neurons in submerged slices of DLM transilluminated to reveal the borders of the nucleus. Slices were continuously perfused with warmed HEPES-free ACSF (28°C–32°C, see below) at a flow rate of 3 ml/min. We used glass micropipettes with resistances ranging from 6–12 MΩ. (Puller P-97, Sutter Instrument Co., Novato, CA). For whole-cell recordings, the internal solution contained 120 mM K-methylsulfate, 10 mM HEPES, 2 mM EGTA, 8 mM NaCl, 2 mM MgATP, 0.3 mM GTP (Na^+ salt), and 1 mM $MgCl_2$, pH 7.2, 274–285 mOsm. For perforated-patch recordings, fresh gramicidin stock solution (0.2–0.3 mg/ml) was prepared in DMSO. The tip of the pipette was filled with internal solution identical to that used in whole-cell configuration. The pipette was then back-filled with solution that contained 134 mM K-methylsulfate, 10 mM HEPES, 0.5 mM EGTA, 8 mM NaCl, 2 mM $MgCl_2$, and gramicidin stock solution for a final concentration of 0.2–0.3 μg/ml (Ding and Perkel, 2002). In three control experiments, 25 mM KCl replaced equimolar K-methlysulfate, to intentionally disrupt the chloride reversal potential upon break-in.

Signals were amplified with an Axoclamp 2B (Axon Instruments, Foster City, CA), in bridge mode, filtered at 3 kHz, then amplified and filtered by an second amplifier (Brownlee Model 410, Brownlee Precision, Santa Clara, CA) before being digitized (National Instruments) and sampled at 6 kHz using custom LabView software written by D.J. Perkel and M.A. Farries. In experiments with random Poisson or natural stimulus patterns, signals were digitized with a Digidata 1322A, and data were acquired using Clampex software (Axon Instruments), 10 kHz sampling rate, 5 kHz low-pass filter cutoff.

Temperature

All Poisson and natural train experiments were conducted at 30°C.

Constant-frequency, patterned train, and rate-transition experiments were performed between 28°C and 30°C. For temperature experiments, we varied the bath temperature between 28°C and 32°C. We extrapolated rebound latencies at warm temperatures by fitting rebound spike latencies measured from at least three temperatures with an exponential ($R^2 > 0.95$, n = 5 cells). We calculated the Q_{10} value by dividing the rebound latency at the cooler temperature by the extrapolated rebound latency at a temperature 10°C warmer.

Stimulus Delivery and Design

A 500 μm diameter, concentric bipolar stimulating electrode (Frederick Haer Co., Bowdoinham, ME) was positioned superficially within the tract of fibers coursing from Area X to DLM, directly anterior to the nucleus (200–600 μm). Afferents were activated with 100 μs pulses, typically 0.2–5 mA in magnitude, controlled by a stimulus isolation unit (Isoflex, AMPI, Jerusalem, Israel).

A set of 65 "Poisson trains" was generated in Matlab 6.5.1 (MathWorks, Natick, MA) by randomly drawing interpulse intervals from a decaying exponential distribution to make up a 3 s stimulus train with a mean rate of 140 Hz. For experiments aimed at determining the reliability of the response, each train was delivered in duplicate to the slice with 30–60 s between each train presentation.

Patterned trains of IPSPs were used to measure the refractory period and maximal spike-transfer efficiency of IPSP-evoked rebound spikes (n = 6). Here we required that rebound events with sodium spikes be evoked in each of five consecutive pauses within the train. Thus our "optimal" stimulus patterns were defined for sustained firing. We then varied the duration of the train and subsequent pause to drive rebound spikes maximally under this criterion.

Natural spike patterns were generated from single-unit data from Area X in the intact animal (in vivo spike data and song oscillograms kindly provided by S. Kojima, N.A. Hessler, and A.J. Doupe, UCSF). Two trains were taken from playback of the bird's own song (n = 5; mean instantaneous rates [reciprocal interspike interval] of 75.8 [SD 52] Hz and 73.6 [SD 22.46] Hz, respectively). One train was taken from the singing animal (n = 6; mean instantaneous rate of 169 [SD 82] Hz). Each stimulus train was delivered between two and four times to each cell.

Data Analysis

We included 31 cells (21 recorded in perforated patch configuration) from 26 animals in the final data set, based on the following criteria: (1) stable baseline resting membrane potential, (2) IPSP waveform included a distinct trough distinguishable from the stimulus artifact, and (3) IPSPs could be evoked reliably with extracellular stimulation; i.e., synaptic recruitment followed trains of shocks to the fiber bundle.

We calculated rebound latency in Poisson trains (Figure 4A) using a correction that eliminated those stimuli less than 20 ms prior to the rebound event for two reasons. First, we rarely observed rebound latencies below 20 ms. Second, it was clear that IPSPs occurring after apparent crossing of spike threshold in Poisson-train experiments did not cause rebound spikes. In experiments using constant-frequency stimulus trains (Figure 4B), rebound spike latency was defined as the time between the stimulus artifact of the last IPSP in the train and the peak of the first rebound spike.

Spike-Triggered Stimulus Averaging

To determine the patterns of stimuli that gave rise to rebound spikes, we measured the time of each stimulus in the Poisson train that occurred during a window 200 ms prior to each rebound spike. When a burst of multiple sodium spikes occurred, only the first spike was included in the analysis.

Cross-Correlations

The rebound spikes elicited by pairs of duplicate trains were compared using cross-correlation routines in Matlab. Rebound spike times were measured as peak time of the sodium spike and discriminated from calcium spikes by spike duration. For cross-correlation analyses, these spike times were represented in a comb function, which was smoothed by convolution with a Gaussian waveform with a width at half-maximal amplitude of 5 ms. The paired traces were then cross-correlated using the built-in cross-correlation function in Matlab. The resultant cross-correlation function was normalized to the autocorrelation of one of the traces of the pair, which by definition is 1. Shuffled spike trains preserved the number of spikes and the interspike interval distribution of each train, but the order of intervals was randomized. Shuffled spike times generated from this procedure were then cross-correlated in the same manner as the actual spike times. For each pair of rebound spikes, the shuffling procedure was performed 150 times. For measurements of jitter between rebound responses to duplicate trains (width at half-max cross-correlation), cross-correlations

were performed on unsmoothed data. Lag values reported are absolute values.

We assessed the quality of the predictions by cross correlating each predicted spike train with each set of rebound spikes elicited by the spike train in vitro. Methods used here were identical to those used for cross-correlations comparing spike times between responses to duplicate Poisson trains. The percent of observed spikes predicted by the model was calculated for each cell at a threshold cutoff that yielded the best approximation of the rate of observed spikes. This requirement constrained the model from overpredicting spikes to boost the percent of observed spikes predicted.

Acknowledgments

We thank Fred Rieke, Michele Solis, Dawn Blitz, Michael Farries, and Sam Gale for thoughtful comments on the manuscript. We are also grateful to Satoshi Kojima, Neal Hessler, and Allison Doupe (UCSF) for generously providing in vivo spike trains used in this study. This work was supported by NIH grants MH066128 (D.J.P.), T-32 GM07108, and F31 NS049732 (A.L.P.), and NIH/NIDCD P30 Core Grant DC04661. Authors are affiliates of the Virginia Merrill Bloedel Hearing Research Center.

Received: August 17, 2004
Revised: November 3, 2004
Accepted: December 9, 2004
Published: April 6, 2005

References

Bal, T., von Krosigk, M., and McCormick, D.A. (1995). Synaptic and membrane mechanisms underlying synchronized oscillations in the ferret lateral geniculate nucleus in vitro. J. Physiol. *483*, 641–663.

Berger, T.W., Robinson, G.B., Port, R.L., and Sclabassi, R.J. (1987). Nonlinear Systems Analysis of the Functional Properties of the Hippocampal Formation. In Advanced Methods of Physiological System Modeling, Volume 1, V.Z. Marmarelis, ed. (Los Angeles, CA: University of Southern California Press).

Blanton, M.G., Lo Turco, J.J., and Kriegstein, A.R. (1989). Whole cell recording from neurons in slices of reptilian and mammalian cerebral cortex. J. Neurosci. Methods *30*, 203–210.

Bottjer, S.W., Miesner, E.A., and Arnold, A.P. (1984). Forebrain lesions disrupt development but not maintenance of song in passerine birds. Science *25*, 901–903.

Brainard, M.S., and Doupe, A.J. (2000a). Interruption of a basal ganglia-forebrain circuit prevents plasticity of learned vocalizations. Nature *404*, 762–766.

Brainard, M.S., and Doupe, A.J. (2000b). Auditory feedback in learning and maintenance of vocal behaviour. Nat. Rev. Neurosci. *1*, 31–40.

Chevalier, G., and Deniau, J.M. (1990). Disinhibition as a basic process in the expression of striatal functions. Trends Neurosci. *13*, 277–280.

Coulter, D.A., Huguenard, J.R., and Prince, D.A. (1989). Calcium currents in rat thalamocortical relay neurons: kinetic properties of the transient, low-threshold current. J. Physiol. *414*, 587–604.

Dave, A.S., and Margoliash, D. (2000). Song replay during sleep and computational rules for sensorimotor vocal learning. Science *290*, 812–816.

Deniau, J.M., and Chevalier, G. (1985). Disinhibition as a basic process in the expression of striatal functions. II. The striato-nigral influence on thalamocortical cells of the ventromedial thalamic nucleus. Brain Res. *334*, 227–233.

Ding, L., and Perkel, D.J. (2002). Dopamine modulates excitability of spiny neurons in the avian basal ganglia. J. Neurosci. *22*, 5210–5218.

Dobrunz, L.E., and Stevens, C.F. (1999). Response of hippocampal synapses to natural stimulus patterns. Neuron *22*, 157–166.

Doupe, A.J., and Konishi, M. (1991). Song-selective auditory circuits in the vocal control system of the zebra finch. Proc. Natl. Acad. Sci. USA *88*, 11339–11343.

Farries, M.A., and Perkel, D.J. (2002). A telencephalic nucleus essential for song learning contains neurons with physiological characteristics of both striatum and globus pallidus. J. Neurosci. *22*, 3776–3787.

Farries, M.A., Ding, L., and Perkel, D.J. (2005). Evidence for "Direct" and "Indirect" pathways through the song system basal ganglia. J. Comp. Neurol. *484*, 93–104.

Foster, E.F., Mehta, R.P., and Bottjer, S.W. (1997). Axonal connections of the medial magnocellular nucleus of the anterior neostriatum in zebra finches. J. Comp. Neurol. *382*, 364–381.

Gauck, V., and Jaeger, D. (2000). The control of rate and timing of spikes in the deep cerebellar nuclei by inhibition. J. Neurosci. *20*, 3006–3016.

Guinan, J.J., and Li, R.Y.S. (1990). Signal processing in brainstem auditory neurons which receive giant endings (calyces of Held) in the medial nucleus of the trapezoid body of the cat. Hear. Res. *49*, 321–334.

Hahnloser, R.H., Kozhevnikov, A.A., and Fee, M.S. (2002). An ultrasparse code underlies the generation of neural sequences in a songbird. Nature *6902*, 65–70.

Hessler, N.A., and Doupe, A.J. (1999). Singing-related neural activity in a dorsal forebrain-basal ganglia circuit of adult zebra finches. J. Neurosci. *19*, 10461–10481.

Isaacson, J.S., and Walmsley, B. (1995). Receptors underlying excitatory synaptic transmission in slices of the rat anteroventral cochlear nucleus. J. Neurophysiol. *73*, 964–973.

Jahnsen, H., and Llinas, R. (1984a). Electrophysiological properties of guinea-pig thalamic neurons: an in vitro study. J. Physiol. *349*, 205–226.

Jahnsen, H., and Llinas, R. (1984b). Ionic basis for the electroresponsiveness and oscillatory properties of guinea-pig thalamic neurones in vitro. J. Physiol. *349*, 227–247.

Jarvis, E.D., and Nottebohm, F. (1997). Motor-driven gene expression. Proc. Natl. Acad. Sci. USA *94*, 4097–4102.

Kim, U., Sanchez-Vives, M.V., and McCormick, D.A. (1997). Functional dynamics of GABAergic inhibition in the thalamus. Science *278*, 130–134.

Kimpo, R.R., Theunissen, F.E., and Doupe, A.J. (2003). Propagation of correlated activity through multiple stages of a neural circuit. J. Neurosci. *23*, 5750–5761.

Leonardo, A. (2004). Experimental test of the birdsong error-correction model. Proc. Natl. Acad. Sci. USA *101*, 16935–16940.

Luo, M., and Perkel, D.J. (1999a). A GABAergic, strongly inhibitory projection to a thalamic nucleus in the zebra finch song system. J. Neurosci. *19*, 6700–6711.

Luo, M., and Perkel, D.J. (1999b). Long-range GABAergic projection in a circuit essential for vocal learning. J. Comp. Neurol. *403*, 68–84.

Luo, M., and Perkel, D.J. (2002). Intrinsic and synaptic properties of neurons in an avian thalamic nucleus during song learning. J. Neurophysiol. *88*, 1903–1914.

Luo, M., Ding, L., and Perkel, D.J. (2001). An avian basal ganglia pathway essential for vocal learning forms a closed topographic loop. J. Neurosci. *21*, 6836–6845.

Lüthi, A., Bal, T., and McCormick, D.A. (1998). Periodicity of thalamic spindle waves is abolished by ZD7288, a blocker of Ih. J. Neurophysiol. *79*, 3284–3289.

Margoliash, D. (1997). Functional organization of forebrain pathways for song production and perception. J. Neurobiol. *33*, 671–693.

McCormick, D.A., and Pape, H.C. (1990). Properties of a hyperpolarization-activated cation current and its role in rhythmic oscillation in thalamic relay neurons. J. Physiol. *431*, 291–318.

Mainen, Z.F., and Sejnowski, T.J. (1995). Reliability of spike-timing in neocortical neurons. Science *268*, 1503–1508.

Parent, M., Lévesque, M., and Parent, A. (2001). Two types of projection neurons in the internal pallidum of primates: single-axon tracing and three-dimensional reconstruction. J. Comp. Neurol. *439*, 162–175.

Porcello, D.M., Smith, S.D., and Huguenard, J.R. (2003). Actions of U-92032, a T-type Ca2+ channel antagonist, support a functional linkage between IT and slow intrathalamic rhythms. J. Neurophysiol. *89*, 177–185.

Scharff, C., and Nottebohm, F. (1991). A comparative study of the behavioral deficits following lesions of various parts of the zebra finch song system: implications for vocal learning. J. Neurosci. *11*, 2896–2913.

Sherman, S.M., and Guillery, R.W. (1998). On the actions that one nerve cell can have on another: Distinguishing "drivers" from "modulators". Proc. Natl. Acad. Sci. USA *95*, 7121–7126.

Sherman, S.M., and Guillery, R.W. (2001). Exploring the Thalamus (San Diego, CA: Academic Press), pp. 263–264.

Sohrabji, F., Nordeen, E.J., and Nordeen, K.W. (1990). Selective impairment of song learning following lesions of a forebrain nucleus in the juvenile zebra finch. Behav. Neural Biol. *53*, 51–63.

Stark, L.L., and Perkel, D.J. (1999). Two-stage, input-specific synaptic maturation in a nucleus essential for vocal production in the zebra finch. J. Neurosci. *19*, 9107–9116.

Thomson, A.M. (1988). Inhibitory postsynaptic potentials evoked in thalamic neurons by stimulation of the reticularis nucleus evoke slow spikes in isolated rat brain slices – I. Neuroscience *25*, 491–502.

Trussell, L.O. (1999). Synaptic mechanisms for coding timing in auditory neurons. Annu. Rev. Physiol. *61*, 477–496.

Ueki, A. (1983). The mode of nigro-thalamic transmission investigated with intracellular recording in the cat. Exp. Brain Res. *49*, 116–124.

Ulrich, D., and Huguenard, J.R. (1997a). GABA(A)-receptor-mediated rebound burst firing and burst shunting in thalamus. J. Neurophysiol. *78*, 1748–1751.

Ulrich, D., and Huguenard, J.R. (1997b). Nucleus-specific chloride homeostasis in rat thalamus. J. Neurosci. *17*, 2348–2354.

Vates, G.E., Vicario, D.S., and Nottebohm, F. (1997). Reafferent thalamo- "cortical" loops in the song system of oscine songbirds. J. Comp. Neurol. *380*, 275–290.

Wild, J.M. (1993). Descending projections of the songbird nucleus robustus archistriatalis. J. Comp. Neurol. *338*, 225–241.

Williams, H., and Mehta, N. (1999). Changes in adult zebra finch song require a forebrain nucleus that is not necessary for song production. J. Neurobiol. *39*, 14–28.

Zhang, S., and Trussell, L.O. (1994). Voltage clamp analysis of excitatory synaptic transmission in the avian nucleus magnocellularis. J. Physiol. *480*, 123–136.

Zhou, N., and Parks, T.N. (1992). Gamma-D-glutamylaminomethyl sulfonic acid (GAMS) distinguishes subtypes of glutamate receptor in the chick cochlear nucleus (nuc. magnocellularis). Hear. Res. *60*, 20–26.